A fast algorithm for simulating finite scattering configurations featuring Rayleigh–Bloch waves

L. G. Bennetts[1] M. Ganesh[2] S. C. Hawkins[3]
M. A. Peter[4]

(Received 17 February 2025; revised 14 August 2025)

Abstract

Rayleigh–Bloch (RB) waves are a class of guided waves that occur in periodic structures, specifically in one-dimensional (1D) arrays of scatterers, and decay exponentially away from the array. RB waves can also be identified on large finite arrays, and contribute significantly to their response to incident wave forcing. Moreover, RB waves can be utilised to design arrays with specific characteristics, such as trapping, blocking, or amplifying waves. However, simulating wave interactions with these arrays poses challenges due to the large number of scatterers. Additionally, the existence of RB waves is linked to poor conditioning of the associated linear systems. We address these challenges by employing a recently developed fast matrix–vector product boundary integral equation algorithm for simulating wave interactions in large

DOI:10.21914/anziamproc.v66.19615, Published 2025-12-08, as part of the Proceedings of the 22nd Biennial Computational Techniques and Applications Conference. ISSN 1445-8810. (Print two pages per sheet of paper.)

configurations. We combine state-of-the-art iterative solvers with effective preconditioners, for periodic structures containing hundreds of penetrable 2D scatterers.

Contents

1 Introduction C80

2 Wave-scattering model C82

3 Boundary-integral and algebraic systems C83

4 Iterative and preconditioned fast solver C85

5 Numerical experiments C86

6 Conclusions C91

1 Introduction

Rayleigh–Bloch (RB) waves are supported by 1D arrays of scatterers embedded in 2D background media. They have been discovered in various contexts, including acoustics, optics, elasticity, and surface water waves [e.g., 4, and references therein]. These waves propagate along the array and decay exponentially away from it. RB waves are classically interpreted as unforced solutions for infinite line arrays of identical and periodically spaced scatterers. They are typically found by searching for solutions with real-valued wavenumbers that exist below a so-called 'cut-off' wavenumber (or frequency) where wave energy cannot escape from the array, and relate to the Bloch conditions of quasi-periodicity along the array [14].

In acoustics, RB waves are found for all wavenumbers below the cut-off when the scatterers are sound-hard [11]. Additionally, generalised RB waves

with complex wavenumbers exist for certain frequencies around the cut-off. These are identified using methodologies different from those applied below the cut-off, including transfer matrices [2], Green's functions [13], and FEM–PML discretisations [4]. RB waves have also been observed for penetrable scatterers [18], which is the focus of this work.

Interest in RB waves arises from their use in interpreting and predicting the response of large finite arrays to incident wave forcing [12, 19, 4, 10]. When they exist, RB waves can be identified as contributing to the response, alongside other wave modes that leak energy away from the array. In general, there are RB waves propagating in both directions along the array and their coherent interactions lead to resonances at specific frequencies. For graded arrays (e.g., slowly varying spacings), RB waves can exist with properties that evolve along the array and the concept of rainbow trapping can be used to amplify the RB waves at desired locations [15, 3, 1]. Frequency regions for which RB waves do not exist are referred to as band gaps, which can be utilised to block wave propagation.

Design of finite arrays can be informed by the RB wavenumbers of the corresponding infinite array [7, 19, 2], simplifying the problem to a single strip. However, for the subsequent optimisation of the finite structure, it is essential to simulate waves within large, finite, and potentially graded arrays, which poses computational challenges. Moreover, a prerequisite for considering graded arrays is to explore and validate algorithms for ungraded arrays first.

A new boundary integral equation-based algorithm for simulating multiple scattering was applied by Ganesh and Hawkins [8] for configurations containing large numbers of scatterers, arranged both regularly and randomly. The challenge of solving large dense linear systems associated with boundary integral equations was addressed using the iterative solver GMRES [17], combined with a fast matrix–vector product algorithm, which relies on the projection of the fields reflected by the scatterers onto wavefunction expansions.

We apply the algorithm of Ganesh and Hawkins [8] to large finite periodic

arrays. The near-singularity of the integral equations, which is linked to the unforced RB wave solutions of the corresponding infinite array, leads to badly conditioned linear systems that are challenging for iterative solvers. We demonstrate that the computational time required to solve the linear systems for large arrays containing more than a thousand scatterers can be reduced to just a few hours. This is achieved through the use of the fast matrix–vector product in conjunction with the iterative solver FGMRES [16] and a block-preconditioner.

2 Wave-scattering model

We consider two-dimensional waves in a plane containing a line array of regularly spaced identical penetrable scatterers with refractive index $\nu \neq 1$. We index the scatterers by the index set $F \subseteq \mathbb{Z}$, so that individual scatterers are $D_J = x_J + D$, where $x_J = (Jd, 0)^T$ is the centre of the Jth scatterer for $J \in F$, and d is a fixed parameter that controls the separation between the scatterers. Here, D represents a template scatterer, and we assume that D is an open set with sufficiently smooth boundary. A sample configuration is visualised in Figure 1.

The scattered field u^s exterior to $D_F = \cup_{J\in F} D_J$ and the interior field u^i inside D_F are excited by a known incident field u^{inc}. All three fields satisfy the Helmholtz equation

$$\Delta u(x) + \kappa(x)^2 u(x) = 0\,, \tag{1}$$

with piecewise-constant wavenumber

$$\kappa(x) = \begin{cases} k & \text{for } x \in \mathbb{R}^2 \setminus \overline{D_F}\,, \\ \nu k & \text{for } x \in D_F\,, \end{cases}$$

where $\overline{D_F}$ denotes the closure of D_F. For finite arrays, the scattered field additionally satisfies the radiation condition [5, eq. (3.108)]. The interior

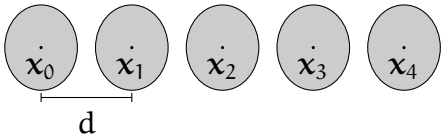

Figure 1: Schematic showing a line array $D_{\{0,\dots,4\}}$ of elliptical particles.

field u^i and exterior field $u^s + u^{inc}$ are coupled through the transmission boundary conditions

$$u^s(x) + u^{inc}(x) = u^i(x)\,, \quad \frac{\partial}{\partial n}(u^s + u^{inc})(x) = \frac{\partial u^i}{\partial n}(x)\,, \quad x \in \partial D_F\,. \tag{2}$$

RB waves are unforced (that is $u^{inc} = 0$) non-trivial solutions of (1)–(2) for the infinite array D_F for $F = \mathbb{Z}$, so that the total field satisfies the quasi-periodicity condition

$$u(x + de_1) = e^{i\beta d} u(x)\,, \quad x \in \mathbb{R}^2\,, \tag{3}$$

where $e_1 = (1, 0)^T$. A consequence of (3) is that these solutions can be studied on the strip $S = (-d/2, d/2) \times \mathbb{R}$, in which case (3) and its analogue for the normal derivatives apply at the strip boundaries. The dispersion relation $\beta = \beta(k)$ can be used to understand the response of large finite arrays. For finite arrays, equation (3) need not hold and it is necessary to model the entire array numerically, which is the focus of this article.

3 Boundary-integral and algebraic systems

For numerical solution of the scattering problem (1)–(2) for a finite array D_F with $F = \{0, \dots, N-1\}$ and fixed wavenumber k, we represent the scattered field using the surface-integral ansatz [8]

$$u^s(x) = \sum_{J \in F} \left(\mathcal{K}_J^0 \psi|_{\partial D_J} + \mathcal{S}_J^0 \phi|_{\partial D_J} \right)(x)\,, \quad x \in \mathbb{R}^2 \setminus \overline{D_F}\,, \tag{4}$$

and the interior field using the local boundary-integral ansatz

$$u^i(x) = \left(\mathcal{K}_J^1 \psi|_{\partial D_J} + \mathcal{S}_J^1 \phi|_{\partial D_J}\right)(x), \quad x \in D_J, \tag{5}$$

for each $J \in Z$, where ψ and ϕ are unknown surface densities defined on ∂D_F whose calculation is addressed below. Here $\mathcal{S}_F^\sigma$ and $\mathcal{K}_F^\sigma$ denote the single- and double-layer potentials, respectively [defined in 5, eqns (3.8)–(3.9), but omitting the factor 2]. The superscripts $\sigma = 0, 1$ indicate that the exterior and interior wavenumber is used in the kernel, respectively.

Following details from Ganesh and Hawkins [8], substituting the ansatz (4)–(5) into the transmission boundary conditions (2) leads to a large boundary-integral system

$$\sum_{J \in F} \mathcal{A}_{IJ} \chi_J = \beta_I, \quad I \in F, \tag{6}$$

where the diagonal and off-diagonal blocks, respectively, are

$$\mathcal{A}_{II} = \begin{pmatrix} \mathcal{I} + \mathcal{K}_I^0 - \mathcal{K}_I^1 & \mathcal{S}_I^0 - \mathcal{S}_I^1 \\ \frac{\partial}{\partial n}(\mathcal{K}_I^1 - \mathcal{K}_I^0) & \mathcal{I} + \frac{\partial}{\partial n}(\mathcal{S}_I^1 - \mathcal{S}_I^0) \end{pmatrix}, \quad \mathcal{A}_{IJ} = \begin{pmatrix} \mathcal{K}_J^0 & \mathcal{S}_J^0 \\ -\frac{\partial}{\partial n}\mathcal{K}_J^0 & -\frac{\partial}{\partial n}\mathcal{S}_J^0 \end{pmatrix}. \tag{7}$$

In the former expression, the operators $\mathcal{K}_I^\sigma$ and $\mathcal{S}_I^\sigma$ are the weakly-singular double- and single-layer operators, whilst in the latter they can be considered surface potentials with smooth kernels. Therefore, it is convenient to break the usual convention by not using different symbols for these. The normal derivatives in (7) should be interpreted as in Theorem 3.1 of Colton and Kress [5]; thus, the operators in the (2,1)-block of A_{II} are the hypersingular operators, but their difference is weakly singular. The solution and right-hand side vectors in (6) are $\chi_J = (\psi|_{\partial D_J}, \phi|_{\partial D_J})$ and $\beta_I = \left(-u^{inc}|_{\partial D_I}, \frac{\partial u^{inc}}{\partial n}|_{\partial D_I}\right)$, respectively.

Following Ganesh and Hawkins [8], we discretise each operator in the system (6) using the Nyström method [5, Sec. 3.6] with $2m$ quadrature points, leading to

$$\sum_{J \in F} A_{IJ} x_J = b_I, \quad I \in F, \tag{8}$$

where A_{IJ}, x_J and b_I are the Nyström discretisations of $\mathcal{A}_{IJ}$, χ_J and β_I, respectively. Each matrix A_{IJ} has dimension $2m \times 2m$.

4 Iterative and preconditioned fast solver

We solve the linear system (8) iteratively using Krylov solvers GMRES [17] and FGMRES [16]. These require matrix–vector products $y_I = \sum_{J=0}^{N-1} A_{IJ} x_J$, $I = 0, \ldots, N-1$, with the matrix in (8). Subsidiary matrix–vector products with the off-diagonal block matrices A_{IJ}, which give fields on ∂D_I coming from ∂D_J, are computed without assembling the matrices, which reduces the memory requirement of the algorithm from $\mathcal{O}(N^2)$ to $\mathcal{O}(N)$.

The CPU time for the matrix–vector product is reduced by projecting the fields radiated by each scatterer ∂D_J onto the basis of radiating wavefunctions $e_l(z) = H_l^{(1)}(k|z|)e^{il\theta(z)}$, for $l = -L, \ldots, L$, where L is the truncation order as determined by Ganesh and Hawkins [9, eq. (12)] and $H_l^{(1)}$ is the Hankel function of the first kind and order l. In particular, we use the projection operator $\mathcal{R}_J \mathcal{R}_J^*$ to approximate

$$\begin{pmatrix} \mathcal{K}_J^0 & \mathcal{S}_J^0 \end{pmatrix} \begin{pmatrix} \psi \\ \phi \end{pmatrix} \approx \mathcal{R}_J \mathcal{R}_J^* \begin{pmatrix} \psi \\ \phi \end{pmatrix}.$$

Here, $\mathcal{R}_J$ is the synthesis operator which maps expansion coefficients $a = (a_l)_{l=-L,\ldots,L}$, to the corresponding radiating field,

$$(\mathcal{R}_J a)(x) = \sum_{l=-L}^{L} a_l e_l(x - x_J). \tag{9}$$

The associated analysis operator $\mathcal{R}_J^*$, which maps the surface potential (ψ, ϕ) to the corresponding expansion coefficients, is described by Ganesh and Hawkins [8].

The main idea is then to project these fields onto the basis of regular wavefunctions $f_l(z) = J_l(k|z|)e^{il\theta(z)}$, for $l = -L, \ldots, L$, locally around each ∂D_I.

Here, J_l is the Bessel function of order l. The synthesis operator, analagous to (9), is

$$(\mathcal{Q}_I a)(x) = \sum_{l=-L}^{L} a_l f_l(x - x_I)\,. \tag{10}$$

The local approximation near ∂D_I is then given by $\mathcal{Q}_I \mathcal{Q}_I^* \mathcal{R}_J \mathcal{R}_J^*$. We do not need to evaluate the analysis operator $\mathcal{Q}_I^*$ numerically because $\mathcal{Q}_I^* \mathcal{R}_J$ is given in closed form by the translation–addition theorem [6]. Thus, our final approximation to the product $\mathcal{A}_{IJ}(\psi, \phi)$ is given by

$$\begin{pmatrix} I \\ \frac{\partial}{\partial n} \end{pmatrix} \begin{pmatrix} \mathcal{K}_J^0 & \mathcal{S}_J^0 \end{pmatrix} \begin{pmatrix} \psi \\ \phi \end{pmatrix} \approx \begin{pmatrix} I \\ \frac{\partial}{\partial n} \end{pmatrix} \mathcal{Q}_I (\mathcal{Q}_I^* \mathcal{R}_J) \mathcal{R}_J^* \begin{pmatrix} \psi \\ \phi \end{pmatrix}. \tag{11}$$

We present results using preconditioned GMRES with a block-Jacobi preconditioner $y_I = A_{II}^{-1} x_I$, for $I = 0, \ldots, N-1$, and with a block-tridiagonal preconditioner defined similarly. Both the block-Jacobi and block-tridiagonal preconditioners can be implemented directly, using LU-factorisation of appropriate diagonal blocks.

We also present results with FGMRES(m), which preconditions GMRES with an inner iteration that uses m steps of GMRES to approximate the solution of the block-pentadiagonal system. This inner GMRES solve is itself preconditioned using the block-tridigonal preconditioner. The key idea is that the block-pentadiagonal matrix is an approximation to the matrix (A_{IJ}), which is much cheaper to apply.

5 Numerical experiments

We present numerical results for arrays of penetrable elliptical particles with refractive index $\nu = 3$, width 1.6 and height 1.88. In all of our numerical experiments, the separation parameter $d = 4$ is fixed.

Dispersion curves for infinite arrays of sound-hard circular particles are computed by Bennetts and Peter [2] using a transfer-matrix method. This

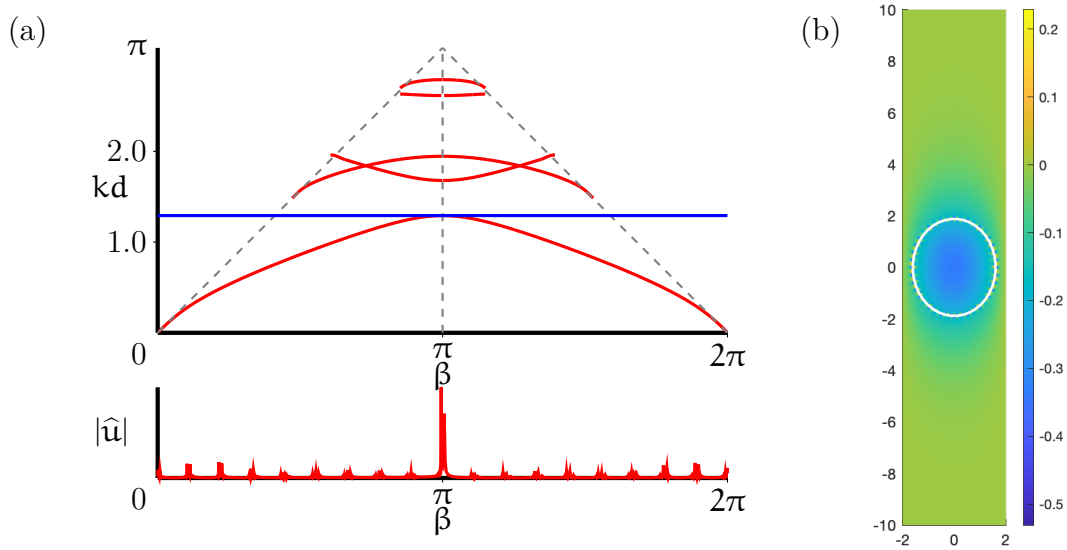

Figure 2: (a) Dispersion curves for an infinite array (top); and frequency response $\hat{u}$ for a finite array with $N = 1024$ scatterers illuminated from the left-hand side by a point source (bottom). RB waves in the infinite array occur at the intersections of the blue line with the red dispersion curves. (b) Visualisation of $\mathrm{Re}\, u$, the total field, in the strip $x_{512} + S$. The size parameter is $kd = 1.292$.

method is extended to penetrable elliptical particles using the T-matrix of the penetrable elliptical particles, which is computed using the TMATSOLVER package [9], and replaces the diagonal T-matrix of the circular particles in [2, eq. (2.8)]. In this way, dispersion curves for the infinite array $D_{\mathbb{Z}}$ are computed accurately and are visualised in Figures 2(a) and 3(a). The sound line (dashed) shows the dispersion relation for waves in free space.

The first and third dispersion curves (as k increases along the sound line) are associated with RB waves that are symmetric about the x-axis. The second dispersion curve is associated with RB waves that are antisymmetric about the x-axis. In the region $kd \in [1.6784, 1.9452]$, there exist both symmetric

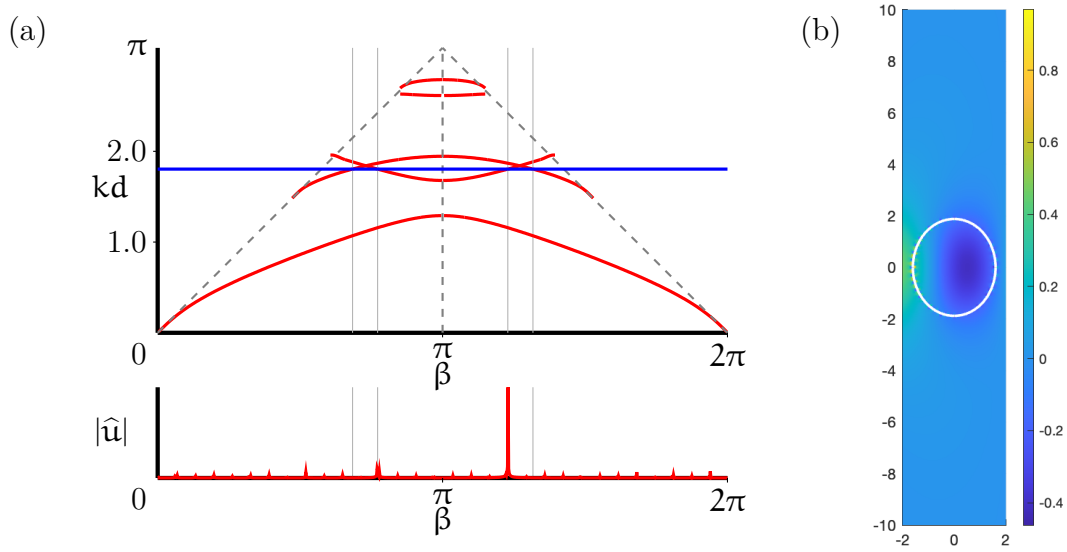

Figure 3: (a) Dispersion curves for an infinite array (top); and frequency response $\hat{u}$ for a finite array with $N = 1024$ scatterers illuminated from the left-hand side by a point source (bottom). RB waves in the infinite array occur at the intersections of the blue line with the red dispersion curves. (b) Visualisation of $\mathrm{Re}\, u$, the total field, in the strip $x_{512} + S$. The size parameter is $kd = 1.804$.

and antisymmetric RB waves. Here, and in what follows, it is convenient to give the wavenumber via the dimensionless parameter kd, and we emphasise again that $d = 4$ is fixed.

Our experiments are focused on simulating the waves corresponding to the RB waves in finite arrays $D_{\{0,\dots,N-1\}}$ for fixed size parameters kd using the method in Sections 3–4. We choose size parameters $kd = 1.292$ (Figure 2) and $kd = 1.804$ (Figure 3) in order to examine near-stationary RB waves (in the former) and propagating symmetric and antisymmetric RB waves (in the latter). In both cases, leftward and rightward-propagating RB waves exist for the corresponding infinite array.

Excitation of RB waves in finite arrays can be examined by spatial–frequency analysis of the field near the array. To that end, we illuminate the finite array $D_{\{0,\dots,N-1\}}$ from the left-hand side using a point source at $(-4,0)$, which excites symmetric RB waves in the array. We evaluate the total field $u(y_j)$ at the equally spaced points $y_j = (jL/(n-1), R)$, $j = 0,\dots,n-1$, which lie on a straight line just above the array. Here, $L = (N-1)d$ is the length of the array. From the vector $(u_j)_{j=0,\dots,n-1}$ of total field values $u_j = u(y_j)$, we compute the vector $(\hat{u}_i)_{i=0,\dots,n-1}$ using the FFT. The entry $\hat{u}_i$ gives the response of the array at spatial frequency $\beta_i = 2\pi di/(hn)$, $i = 0,\dots,n-1$, where $h = L/(n-1)$ is the sampling frequency and n is chosen so that we have ten points per wavelength along the line. The frequency resolution is proportional to N so that where dispersion curves are close together or close to the sound line, large N is required to identify the dispersion curves.

In Figures 2(a) and 3(a), we plot the normalised frequency response $\hat{u}$ induced in the finite arrays for $kd = 1.292$ and $kd = 1.804$, respectively, for $N = 1024$. The peaks in $\hat{u}$ are clearly associated with the symmetric RB waves identified by the dispersion curves. Similar results are obtained for smaller N but the lower β-resolution in that case leads to less well defined peaks.

In Figures 2(b) and 3(b), we visualise the total field near the centre of the array in the strip $x_{512} + S$ for $N = 1024$. In both cases, the field is a close match to the corresponding RB wave mode of the infinite array (not shown). In the case of $kd = 1.292$, the selected wavenumber is very close to the cut-off wavenumber so both modes are almost identical to the stationary mode, which is commonly called the Dirichlet mode because it can be identified with the mode in the strip satisfying homogeneous Dirichlet boundary conditions on the strip boundary [12]. In the case of $kd = 1.804$, the field is dominated by the rightward symmetric mode.

In Figure 4 (left) we plot the CPU time required for a single matrix–vector product with the matrix (A_{IJ}) to demonstrate the approximately 40-times reduction in CPU time obtained using the approximation in (11). The wavenumber is $kd = 1.804$ and all CPU times are obtained in serial using Matlab

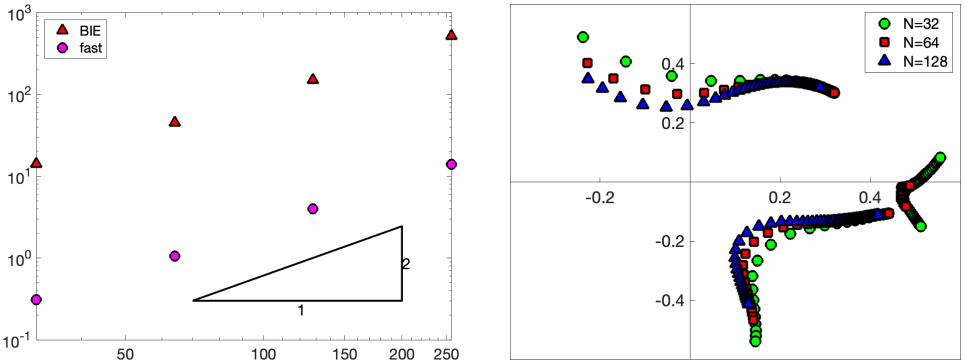

Figure 4: (Left) CPU time plotted against N for a single matrix–vector product with the matrix (A_{IJ}) using the fast projection-based method in Section 4 (fast) and applying a standard quadrature evaluation method in the boundary integral equation system (6)–(7) (BIE), for the finite array $D_{\{0,\ldots,N-1\}}$ with $kd = 1.804$. (Right) 100 smallest-modulus eigenvalues of the matrix (A_{IJ}) for the finite array $D_{\{0,\ldots,N-1\}}$ for $N = 32, 64, 128$.

on a server with 2.5 GHz processors. Results by Ganesh and Hawkins [8] demonstrate further speedup for configurations with fixed width using the Fast Multipole Method (FMM). However, the line arrays in this work have width L (and acoustic size-parameter kL) proportional to N so that the efficiency of the FMM with respect to N cannot be realised in this case.

Finally, in Table 1, we demonstrate the efficiency of the different preconditioning strategies by tabulating the number of iterations and CPU time required to reduce the residual norm by a factor of 10^{-4} for $kd = 1.804$. The large number of iterations required and their approximately $\mathcal{O}(N)$-growth demonstrate the tremendous difficulty of these linear systems. However, the preconditioning strategies are effective and FGMRES(5) demonstrates roughly 50% reduction in the CPU time compared with no preconditioning. Qualitatively similar results were obtained for $kd = 1.292$.

The ill-conditioning in the linear system is associated with the excitation of RB

Table 1: Solver iterations and CPU time (in minutes) for configurations with N scatterers illuminated by an external point source with size parameter kd = 1.804. A × indicates no convergence within 2000 iterations.

		GMRES						FGMRES(5)	
		None		Jacobi		Tridiagonal		Tridiagonal	
N	kL	itns	CPU	itns	CPU	itns	CPU	itns	CPU
32	55.9	176	1.0	91	0.5	49	0.3	42	0.5
64	113.7	348	6.9	182	3.8	95	2.0	70	2.4
128	229.1	689	52.9	370	28.6	186	14.3	130	13.4
256	460.0	1376	402.5	752	220.3	369	108.1	243	84.6
512	921.8	×	2328.2	1534	1794.9	739	844.7	474	598.5
1024	1845.5	×	9012.9	×	9008.5	1478	6645.4	897	4212.7

waves by the illuminating point source. When the exterior forcing is replaced by an interior point source which is not associated with RB waves [8, eq. (40)], the iteration counts for FGMRES(5) in the $N = 1024$ case reduce to 49 and 59 for $kd = 1.292$ and $kd = 1.804$, respectively. In Figure 4 (right), we plot the 100 smallest-modulus eigenvalues of the finite array for $N = 32, 64, 128$ to demonstrate that the smallest eigenvalues converge towards the origin as N increases. This is expected, and, indeed, the RB waves are associated with zero eigenvalues of the associated infinite-dimensional operator.

6 Conclusions

In this work, we have investigated an approach for simulating wave interactions with large finite regular arrays that feature RB waves. Our approach utilises state-of-the-art iterative solvers with a fast matrix–vector product algorithm and effective preconditioners to address challenges arising from the large number of scatterers and poor conditioning of the linear systems, which is associated with the RB waves. Simulations of wave interactions with such finite regular arrays is a key step in the theoretical study of RB waves in

infinite arrays. In future work, we will extend our method to large graded finite arrays to demonstrate amplification of the wave field associated with rainbow trapping. It is envisaged that amplification of the wave field in this way will have applications in energy harvesting.

Acknowledgements The authors thank two anonymous reviewers for their valuable suggestions to improve this article. SCH and MG gratefully acknowledge the support of the Australian Research Council (ARC) Discovery Project Grant (DP220102243). MG was supported by the Simons Foundation through Grant No. 51882. LGB is supported by the ARC (FT190100404, DP240100325).

References

[1] A. J. Archer, H. A. Wolgamot, J. Orszaghova, L. G. Bennetts, M. A. Peter, and R. V. Craster. "Experimental realisation of broadband control of water wave energy amplification in chirped arrays". In: *Phys. Rev. Fluids* 5 (2020), 062801(R). DOI: 10.1103/PhysRevFluids.5.062801 (cit. on p. C81).

[2] L. G. Bennetts and M. A. Peter. "Rayleigh–Bloch waves above the cutoff". In: *J. Fluid Mech.* 940 (2022), A35. DOI: 10.1017/jfm.2022.247 (cit. on pp. C81, C86, C87).

[3] L. G. Bennetts, M. A. Peter, and R. V. Craster. "Graded resonator arrays for spatial frequency separation and amplification of water waves". In: *J. Fluid Mech.* 854 (2018), R4. DOI: 10.1017/jfm.2018.648 (cit. on p. C81).

[4] G. J. Chaplain, S. C. Hawkins, M. A. Peter, L. G. Bennetts, and T. A. Starkey. "Acoustic lattice resonances and generalised Rayleigh–Bloch waves". In: *Nature Comm. Phys.* 8, 37 (2025). DOI: 10.1038/s42005-025-01950-4 (cit. on pp. C80, C81).

[5] D. Colton and R. Kress. *Inverse Acoustic and Electromagnetic Scattering Theory*. 4th. Springer, 2019. DOI: 10.1007/978-3-030-30351-8 (cit. on pp. C82, C84).

[6] T. J. Dufva, J. Sarvas, and J. Sten. "Unified derivation of the translation addition theorems for the spherical and vector wave functions". In: *Prog. in Electromag. Res. B* 4 (2008), pp. 79–99. DOI: 10.2528/PIERB07121203 (cit. on p. C86).

[7] D. V. Evans and R. Porter. "Trapping and near-trapping by arrays of cylinders in waves". In: *J. Eng. Math.* 35 (1999), pp. 149–179. DOI: 10.1023/A:1004358725444 (cit. on p. C81).

[8] M. Ganesh and S. C. Hawkins. "A fast algorithm for the two-dimensional Helmholtz transmission problem with large multiple scattering configurations". In: *J. Acoust. Soc. Am.* 156 (2024), pp. 752–762. DOI: 10.1121/10.0028121 (cit. on pp. C81, C83, C84, C85, C90, C91).

[9] M. Ganesh and S. C. Hawkins. "Algorithm 975: TMATROM—A T-matrix reduced order model software". In: *ACM Trans. Math. Softw.* 44 (2017), 9:1–9:18. DOI: 10.1145/3054945 (cit. on pp. C85, C87).

[10] S. C. Hawkins, L. G. Bennetts, M. A. Nethercote, M. A. Peter, Daniel Peterseim, H. J. Putley, and B. Verfürth. "Metamaterial applications of TMATSOLVER, an easy-to-use software for simulating multiple wave scattering in two dimensions". In: *Proc. Roy. Soc. A* 480, 2292 (2024). DOI: 10.1098/RSPA.2023.0934 (cit. on p. C81).

[11] C. M. Linton and M. McIver. "The existence of Rayleigh–Bloch surface waves". In: *J. Fluid Mech.* 470 (2002), pp. 85–90. DOI: 10.1017/S0022112002002227 (cit. on p. C80).

[12] H. D. Maniar and J. N. Newman. "Wave diffraction by a long array of cylinders". In: *J. Fluid Mech.* 339 (1997), pp. 309–330. DOI: 10.1017/S0022112097005296 (cit. on pp. C81, C89).

[13] K. Matsushima, L. G. Bennetts, and M. A. Peter. "Tracking Rayleigh–Bloch waves swapping between Riemann sheets". In: *Proc. Roy. Soc. A* 480, 2301 (2024). DOI: 10.1098/rspa.2024.0211 (cit. on p. C81).

[14] R. Porter and D. V. Evans. "Rayleigh–Bloch surface waves along periodic gratings and their connection with trapped modes in waveguides". In: *J. Fluid Mech.* 386 (1999), pp. 233–258. DOI: 10.1017/S0022112099004425 (cit. on p. C80).

[15] V. Romero-Garcia, R Picó, A. Cebrecos, V. J. Sánchez-Morcillo, and K. Staliunas. "Enhancement of sound in chirped sonic crystals". In: *Appl. Phys. Lett.* 102, 091906 (2013). DOI: 10.1063/1.4793575 (cit. on p. C81).

[16] Y. Saad. "A Flexible Inner-Outer Preconditioned GMRES Algorithm". In: *SIAM J. Sci. Comp.* 14.2 (1993), pp. 461–469. DOI: 10.1137/0914028 (cit. on pp. C82, C85).

[17] Y. Saad and M. H. Schultz. "GMRES: A generalized minimal residual algorithm for solving nonsymmetric linear systems". In: *SIAM J. Sci. Stat. Comput.* 7.3 (1986), pp. 856–869. DOI: 10.1137/0907058 (cit. on pp. C81, C85).

[18] I. Thompson and C. M. Linton. "Guided surface waves on one- and two-dimensional arrays of spheres". In: *SIAM J. Appl. Math.* 70 (2010), pp. 2975–2995. DOI: 10.1137/100787519 (cit. on p. C81).

[19] I. Thompson, C. M. Linton, and R. Porter. "A new approximation method for scattering by long finite arrays". In: *Q. J. Mech. Appl. Math.* 61 (2008), pp. 333–352. DOI: 10.1093/qjmam/hbn006 (cit. on p. C81).

Author addresses

1. **L. G. Bennetts**, School of Mathematics and Statistics, University of Melbourne, Parkville VIC 3010, Australia.

orcid:0000-0001-9386-7882

2. **M. Ganesh**, Department of Applied Mathematics and Statistics, Colorado School of Mines, Golden, Colorado 80410, USA.
orcid:0000-0002-7792-4119

3. **S. C. Hawkins**, School of Mathematical and Physical Sciences, Macquarie University, New South Wales 2109, Australia.
mailto:stuart.hawkins@mq.edu.au
orcid:0000-0003-1642-613X

4. **M. A. Peter**, Institute of Mathematics and Centre for Advanced Analytics and Predictive Sciences, University of Augsburg, 86135 Augsburg, Germany.
orcid:0000-0001-6107-9806